Design and Characterization of A Synthetic Electron-Transfer Protein

Anna Y. Kornilova,[‡] James F. Wishart,[†] Wenzhong Xiao,[¶] Robin C. Lasey,[‡] Anna Fedorova,[‡] Yeon-Kyun Shin,[¶] and Michael Y. Ogawa*[,‡]

Department of Chemistry and Center for Photochemical Sciences, Bowling Green State University, Bowling Green, Ohio 43403, Chemistry Department, Brookhaven National Laboratory, Upton, New York 11973, and Department of Chemistry and Division of Structural Biology, Lawrence Berkeley Laboratory, University of California, Berkeley, California 94720

Received February 18, 2000

Abstract: A 30-residue polypeptide [H21(30-mer)] with the sequence Ac-K(IEALEGK)$_2$(IEALEHK)-(IEALEGK)G-NH$_2$ was synthesized. The circular dichroism (CD) spectrum of the peptide shows minima at 208 and 222 nm and $\theta_{222}/\theta_{208} = 1.06$, which indicates the formation of a self-assembled coiled-coil when dissolved in aqueous solution. The concentration dependence of the CD data can be fit to an expression that describes a two-state monomer−dimer equilibrium for the apopeptide ($K_d = 1.5 \pm 0.4$ μM and $\theta_{max} = -23\,800 \pm 130$ deg cm^2 dmol^{-1}), showing that it has a maximum helicity of 69%. A [MTSL-C21(30-mer)] dimer was also prepared in which MTSL is the thiol-specific nitroxide spin label 1-oxyl-2,2,5,5-tetramethyl-Δ^3-pyrroline-3-methyl-methanethiosulfonate attached to C21 of the 30-mer. Fourier deconvolution analysis of the dipolar line broadening of the electron paramagnetic resonance (EPR) spectrum yields a measure of the interchain C_α−C_α distance of 13.5 ± 0.9 Å at position 21 of the coiled-coil, which is nearly identical to those distances observed for the isostructural family of bZip proteins. Two metallohomodimers, [Ru(trpy)(bpy)-H21(30-mer)]$_2$ and [Ru(NH$_3$)$_5$-H21(30-mer)]$_2$, in which the ruthenium complexes were coordinated with the H21 site of the 30-mer, were prepared. Sodium dodecyl sulfate−polyacrylamide gel electrophoresis (SDS−PAGE), chemical cross-linking studies, and analytical ultracentrifugation show that the peptides exist as a dimeric coiled-coil with a molecular weight of ∼7.5 kDa. The electron transfer (ET) heterodimer, [Ru(trpy)(bpy)-H21(30-mer)]/[Ru(NH$_3$)$_5$-H21(30-mer)], was prepared, and molecular modeling shows that the two metal complexes are separated by a metal-to-metal distance of ∼24 Å across the noncovalent peptide interface. Pulse radiolysis was used to measure an ET rate constant of $k_{et} = 380 \pm 80$ s^{-1} for the intracomplex electron transfer ($\Delta G^\circ = -1.11$ eV) from the Ru^{II}(NH$_3$)$_5$-H21 donor to the Ru^{III}(trpy)(bpy)-H21 acceptor. The value for k_{et} falls within the range reported for modified proteins over comparable distances and supersedes the one reported in an earlier communication.

Introduction

Protein-based electron-transfer (ET) reactions have been the focus of considerable interest because of their important role in biological energy conversion.[1−4] A central goal of this research is to identify the role, if any, of the intervening protein matrix in propagating long-range donor/acceptor interactions. To this end, much work has been done to investigate the ET properties of photosynthetic reaction centers,[3b,5] surface-derivatized proteins,[4,6] protein−protein complexes,[7−10] and peptide-based model compounds.[1] The last approach to this problem includes the study of intramolecular ET reactions that occur within appropriately derivatized α-helices,[11−13] proline helices,[14−17] artificial β-strands,[18] β-sheets,[19,20] and multihelical bundles.[21−24] However, the design of these first-generation peptide-based ET

‡ Bowling Green State University.
† Brookhaven National Laboratory.
¶ University of California.

(1) For a review, see Ogawa, M. Y. in *Multimetallic and Macromolecular Photochemistry*; Ramamurthy, V., Schanze, K. S., Eds.; Marcel Dekker: New York, 1999; pp 113−150.

(2) *Photochemistry and Radiation Chemistry, Complementary Methods for the Study of Electron-Transfer*; Wishart, J. F.; Nocera, D. G., Eds.; ACS Advances in Chemistry Series 254; American Chemical Society: Washington, DC, 1998.

(3) a) Moser, C. C.; Page, C. C.; Farid, R.; Dutton, P. L. *J. Bioenerg. Biomembr.* **1995**, *27*, 263. (b) Moser, C. C.; Keske, J. M.; Warncke, K.; Farid, R. S.; Dutton, P. L. *Nature* **1992**, *355*, 796.

(4) (a) Winkler, J. R.; Gray, H. B. *J. Biol. Inorg. Chem.* **1997**, *2*, 399. (b) Gray, H. B.; Winkler, J. R. *Annu. Rev. Biochem.* **1996**, *65*, 537.

(5) *The Photosynthetic Reaction Center*, Deisenhofer, J.; Norris, J. R., Eds.; Academic: New York, 1993.

(6) (a) Wishart, J. F.; Sun, J.; Cho, M.; Su, C.; Isied, S. S. *J. Phys. Chem. B* **1997**, *101*, 687. (b) Sun, J.; Wishart, J. F.; Gardineer, M. B.; Cho, M. P.; Isied, S. S. *Inorg. Chem.* **1995**, *34*, 3301. (c) Isied, S. S.; Kuehn, C.; Worosila, G. *J. Am. Chem. Soc.* **1984**, *106*, 1722.

(7) Qiao, T. C.; Witkowski, R.; Henderson, R. McLendon G. *JBIC* **1996**, *1*, 432.

(8) (a) Zhou, J. S.; Hoffman, B. M. *Science* **1994**, *265*, 1693. (b) Stemp, E. D. A.; Hoffman, B. M. *Biochemistry* **1993**, *32*, 10848.

(9) Mei, H.; Wang, K.; Peffer, N.; Weatherly, G.; Cohen, D. S.; Miller, M.; Pielak, G.; Durham, B.; Millett, F. *Biochemistry* **1999**, *38*, 6846.

(10) Olesen, K.; Ejdeback, M.; Crnogorac, M. M.; Kostic, N. M.; Hansson, O. *Biochemistry* **1999**, *38*, 16 695.

(11) (a) For a review, see Sisido, M. *Adv. Photochem.* **1997**, *22*, 197. (b) Kuragaki, M.; Sisido, M. *J. Phys. Chem.* **1996**, *100*, 16 019.

(12) (a) Fox, M. A.; Galoppini, E. *J. Am. Chem. Soc.* **1997**, *119*, 5277. (b) Galoppini, E.; Fox, M. A. *J. Am. Chem. Soc.* **1996**, *118*, 2299.

(13) (a) Basu, G.; Anglos, D.; Kuki, A. *Biochemistry* **1993**, *32*, 3067. (b) Basu, G.; Kubasik, M.; Anglos, D.; Kuki, A. *J. Phys. Chem.* **1993**, *97*, 3956.

(14) (a) Isied, S. S.; Ogawa, M. Y.; Wishart, J. F. *Chem. Rev.* **1993**, *92*, 381. (b) Ogawa, M. Y.; Wishart, J. F.; Young, Z.; Miller, J. R.; Isied, S. S. *J. Phys. Chem.* **1993**, *97*, 11 456. (c) Ogawa, M. Y.; Moreira, I.; Wishart, J. F.; Isied, S. S. *Chem. Phys.* **1993**, *176*, 589.

(15) (a) Schanze, K. S.; Cabana, L. A. *J. Phys. Chem.* **1990**, *94*, 2740. (b) Cabana, L.; Schanze, K. *Adv. Chem. Ser.* **1990**, *226*, 101.

(16) (a) DeFilippis, M. R.; Faraggi, M.; Klapper, M. H. *J. Am. Chem. Soc.* **1990**, *112*, 5640. (b) Faraggi, M.; DeFilippis, M. R.; Klapper, M. H. *J. Am. Chem. Soc.* **1989**, *111*, 5141.

10.1021/ja0006954 CCC: $19.00
Published on Web 08/08/2000

models suffers from the following limitation: whereas many in vivo ET reactions occur across the noncovalent interface of a protein−protein complex, the early model compounds all used peptide bridges to form a covalent link between their donor and acceptor sites. The structural features of these model systems are thus inherently different from those often found in the native biological environment. We describe here a new approach toward the design of more nativelike ET models in which self-organized peptide assemblies are used to separate metal-based redox sites across a well-defined, yet noncovalent, peptide−peptide interface. Future study of these synthetic redox proteins should produce valuable insight into the mechanisms of biological ETs.

The synthesis of the self-assembled peptide−peptide ET complex is derived from recent advances in the rational design of artificial peptide assemblies that retain nativelike structures. A notable example of de novo designed proteins can be seen within the family of synthetic, two-stranded α-helical coiled-coils.[25,26] This ubiquitous protein structure results from the noncovalent self-assembly of two α-helices to form a left-handed supercoil. Synthetic coiled-coils can be constructed from polypeptides whose sequence is based on a seven-residue repeat, $(abcdefg)_n$, in which positions *a* and *d* are occupied by hydrophobic amino acids, *e* and *g* are filled by oppositely charged residues, and *b*, *c*, and *f* denote hydrophilic residues (Figure 1a). This design creates a hydrophobic face of an α-helix to serve as a noncovalent dimerization site for the coiled-coil (Figure 1b). The current study utilizes this motif to prepare a unique, coiled-coil protein designated H21(30-mer) on which metal-based redox sites are positioned to create a synthetic metalloprotein that can exhibit long-range ET. The physicochemical characterization of this protein is presented, along with the results of electron-pulse radiolysis experiments that demonstrate the occurrence of a unimolecular ET reaction (k_{et} = 380 ± 80 s^{-1}) occurring over a metal-to-metal distance of ca. 24 Å across the noncovalent interface.

Experimental

Materials. The Fmoc-protected L-amino acids, diisopropylcarbodiimide, and 1-hydroxybenzotriazole were purchased from Peptides International. *N*-*N*′-Dimethylformamide, dichloromethane, ethylene glycol, and trifluoracetic acid were obtained from Fisher Scientific. Piperidine, anisole, and $[Ru(NH_3)_5Cl]Cl_2$ were purchased from Lancaster Chemicals, Baker Chemicals, and Strem International, respectively. The 2,2′:6′,2″-terpyridine (trpy), 2,2′-bipyridine (bpy), and $RuCl_3{\cdot}H_2O$ were obtained from Aldrich Chemical Company. The thiol-specific MTSL spin-label (MTSL = 1-oxyl-2,2,5,5-tetramethyl-Δ^3-pyrroline-3-methyl-methanethiosulfonate) was purchased from Toronto Research Chemicals Inc. All chemicals and solvents were used as received without further purification.

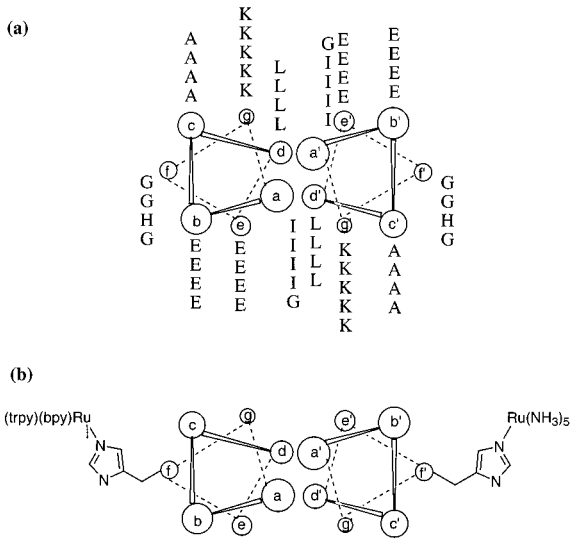

Figure 1. (a) Wheel representation showing the sequence of the H21-(30-mer) protein. (b) Schematic representation of the third heptad repeat of the ET metalloheterodimer.

General Methods. Reversed-phase high-performance liquid chromatography (HPLC) analyses were performed on a Whatman Magnum 9 (500 × 9.4 mm) semipreparative Partisil ODS-3 C_{18} column. A single-pump system was used (Waters model 510) equipped with a binary gradient controller (Autochrom. Inc.) and a Waters model 994 diode array detector/spectrophotometer with a 1-cm cell path length. For preparative separations, the monitoring wavelengths were set to the tails of the absorption bands of the desired compounds. The purity of the resulting samples was subsequently verified by analytical HPLC runs from which the full ultraviolet−visibile (UV−vis) spectra could be obtained. Gel filtration was carried out on columns packed with Bio-Gel P-2 resin (Bio-Rad). The UV−vis spectra of the purified compounds were recorded on a Hewlett-Packard model 8452A diode array spectrophotometer. The molar extinction coefficient, ϵ(478 nm) = 8800 M^{-1} cm^{-1}, was used to determine the concentration of the Ru(trpy)(bpy)-H21(30-mer) peptide.[27] Mass spectral (MS) data were obtained by the Core Protein Facilities of the University of Michigan (Ann Arbor, MI) and the Mass Spectrometry Center of the University of Maryland (College Park, MD). Cyclic voltammetry (CV) was conducted on a BAS 100W Electrochemical Analyzer using a small-volume (200 μL) sample cell equipped with a platinum working electrode, a platinum wire auxiliary electrode, and a $Ag/AgNO_3$ reference electrode. The samples were dissolved in 50 mM phosphate buffer (pH 7.0).

Synthesis of the H21(30-mer) Peptide. The 30-residue polypeptide, with the sequence Ac-K$(IEALEGK)_2$-(IEALEHK)-(IEALEGK)G-NH_2, was synthesized on a Perseptive Biosystems model 9050 Plus Pep-Synthesizer (Framingham, MA) using the fluorenylmethoxycarbonyl N-terminal protection strategy and the manufacturer's PAL PEG-PS resin. Activation was achieved using diisopropylcarbodiimide (DIPCDI) and 1-hydroxybenzotriazole (HOBT) with a 60-min cycle time. This polypeptide is designated H21(30-mer).

Prior to cleavage from the resin, the peptide was N-acetylated with a capping solution containing 0.5 M acetic anhydride, 0.125 M *N*,*N*-diisopropylethylamine (DIEA), and 0.015 M HOBT in dimethylformamide (DMF). Cleavage of the H21(30-mer) from the resin and

(17) (a) McCafferty, D. G.; Friesen, D. A.; Danielson, E.; Wall, C. G.; Saderholm, M. J.; Erickson, B. W.; Meyer. T. J. *Proc. Natl. Acad. Sci., U.S.A.* **1996**, *93*, 8200. (b) Mecklenburg, S. L.; McCafferty, D. G.; Schoonover, J. R.; Peek, B. M.; Erickson, B. W.; Meyer, T. J. *Inorg. Chem.* **1994**, *33*, 2974.

(18) Fernando, S. R. L.; Kozlov, G. V.; Ogawa, M. Y. *Inorg. Chem.* **1998**, *37*, 1900.

(19) Gretchikhine, A. B.; Ogawa, M. Y. *J. Am. Chem. Soc.* **1996**, *118*, 1543.

(20) Williamson, D. A.; Bowler, B. E. *J. Am. Chem. Soc.* **1998**, *120*, 10902.

(21) Kozlov, G. V.; Ogawa, M. Y. *J. Am. Chem. Soc.* **1997**, *119*, 8377.

(22) (a) Mutz, M. W.; Case, M. A.; Wishart, J. F.; Ghadiri, M. R.; McLendon, G. L. *J. Am. Chem. Soc.* **1999**, *121*, 858. (b) Zhou, J; Case, M. A.; Wishart, J. F.; McLendon G. L. *J. Phys. Chem. B* **1998**, *102*, 9975. (c) Mutz, M. W.; McLendon, G. L.; Wishart, J. F.; Gaillard, E. R.; Corin, A. F. *Proc. Natl. Acad. Sci., U.S.A.* **1996**, *93*, 9521.

(23) Rau, H. K.; DeJonge, N.; Haehnel, W. *Proc. Natl. Acad. Sci., U.S.A.* **1998**, *95*, 11526.

(24) Jones, G., II; Vullev, V.; Braswell, E. H.; Zhu, D. *J. Am. Chem. Soc.* **2000**, *122*, 388.

(25) (a) For a review, see Hodges, R. S. *Biochem. Cell Biol.* **1996**, *74*, 133. (b) Zhou, N. E.; Zhu, B. Y.; Kay, C. M.; Hodges, R. S. *Biopolymers* **1992**, *32*, 419.

(26) Graddis, T. J.; Myszka, D. G.; Chaiken, I. M. *Biochemistry* **1993**, *32*, 12664.

(27) (a) Di Bilio, A. J.; Dennison, C.; Gray, H. B.; Ramirez, B. E.; Sykes, A. G.; Winkler, J. R. *J. Am. Chem. Soc.* **1998**, *120*, 7551. (b) Di Bilio, A. J.; Hill, M. G.; Bonander, N.; Karlsson, B. G.; Villahermosa, R. M.; Malmstrom, B. G.; Winkler, J. R.; Gray, H. B. *J. Am. Chem. Soc.* **1997**, *119*, 9921.

deprotection of the amino acid side chains were achieved by gently stirring the resin in a mixture of 88% (v/v) trifluoroacetic acid, 5% (v/v) phenol, 2% (v/v), triisopropylsilane and 5% (v/v) water for 2 h. The crude peptide was then precipitated in cold diethyl ether, collected by vacuum filtration, and dried under vacuum. Final purification was achieved by semipreparative reversed-phase C_{18} HPLC with a linear AB gradient of 1% (v/v) A/min, at a flow rate of 2 mL/min, in which solvent A was 0.1% (v/v) trifluoroacetic acid in acetonitrile and solvent B was 0.1% (v/v) trifluoroacetic acid in water. The collected peptide was then lyophilized and analyzed by MALDI-TOF MS (*m*/*z* obsd: 3287.8, calcd for $[M + H^+]$: 3287.8).

Synthesis of the Spin-Labeled Peptide. The 30-residue polypeptide, C21(30-mer), with the sequence Ac-K(IEALEGK)$_2$-(IEALECK)-(IEALEGK)G-NH_2, was synthesized and purified as just described. A 10-mg (3-μmol) sample of the purified peptide was then dissolved in 2 mL of 50 mM phosphate buffer (pH 7.0) to which a 5-fold molar excess of the thiol-specific MTSL spin-label was added (MTSL = 1-oxyl-2,2,5,5-tetramethyl-Δ^3-pyrroline-3-methyl-methanethiosulfonate). The reaction mixture was stirred at room temperature for 3 h after which it was purified by semipreparative reversed-phase C_{18} HPLC as already described. The collected peptide was then lyophilized and analyzed by MS (*m*/*z* obsd: 3398.9, calcd for $[M + 4H^+]$: 3399.1).

Synthesis of Ru(trpy)(bpy)-H21(30-mer). To a 10-mg (3-μmol) sample of H21(30-mer) dissolved in 2 mL of argon-purged 50 mM phosphate buffer (pH 7.0) was added a concentrated (8−10 mM) solution of $[Ru(trpy)(bpy)Cl]^+$ [28] dissolved in either water or phosphate buffer. The solution was then adjusted to pH 7.7−7.8 and stirred under reduced light for 3 days at 30 °C. The progress of the reaction was monitored by HPLC, which showed the growth of an absorption band centered at 478 nm for the HPLC peak corresponding to the H21(30-mer). After the reaction was complete, the solution was concentrated to a small volume by rotary evaporation and passed through a size-exclusion column equilibrated with water. The metallopeptide solution was then concentrated to near dryness and lyophilized. HPLC analysis showed the existence of a small amount (~5%) of free metal complex in the presence of the desired metallopeptide.

Synthesis of Ru(NH$_3$)$_5$-H21(30-mer). A 15-mg (34-μmol) sample of $[Ru(NH_3)_5Cl](TFA)_2$ was dissolved in 0.5 mL of water, and the resulting solution was purged with argon for 20 min to remove oxygen. A piece of zinc amalgam was then placed into the solution and the solution was bubbled with argon for another 20 min. This solution was then cannulated into a separate flask containing 10 mg (3 μmol) of H21(30-mer) dissolved in 3 mL of argon-saturated 50 mM phosphate buffer. The reaction mixture was stirred under an argon atmosphere overnight, after which it was filtered and injected directly onto the semipreparative HPLC column.

Pulse Radiolysis Measurements. Pulse radiolysis transient absorption experiments were performed on the 2 MeV Van de Graaff accelerator at Brookhaven National Laboratory with a PC-controlled, CAMAC-based control and data acquisition system. The optical detection system consisted of either a pulsed or continuous wave (CW) xenon arc lamp, or a tungsten lamp, appropriate long-pass optical filters, quartz radiolysis cells with various path lengths (2.0 and 6.1 cm), a monochromator, and photomultiplier tube. Digitizer traces were fit to single or double first-order kinetics by nonlinear least-squares methods. Azide radical, $N_3^\bullet$, was produced by the reaction of radiolytically generated hydroxyl radical ($OH^\bullet$) with the azide ion present in the N_2O-saturated water:

$$H_2O \xrightarrow{2\ \text{MeV electrons}} e^-_{aq},\ OH^\bullet,\ H^\bullet,\ H_2,\ H_2O_2 \qquad (1)$$

$$e^-_{aq} + N_2O + H_2O \rightarrow N_2 + OH^\bullet + OH^- \qquad (2)$$

$$OH^\bullet + N_3^- \rightarrow N_3^\bullet + OH^- \qquad (3)$$

Radiolytic dose levels were calculated for each shot based on the current delivered and a calibration factor obtained from the $(SCN)_2^-$ dosimeter ($G = 6.13$, $\epsilon = 7950$ at 472 nm). The yield of $N_3^\bullet$ radicals (G value) was assumed to be 6.0 per 100 eV absorbed. The concentration of $N_3^\bullet$ radicals in each shot was 5−15% of the ruthenated peptide concentration.

Solutions for pulse radiolysis were prepared by reducing a stock solution of equal mole quantities of the $[Ru^{II}(trpy)(bpy)$-H21(30-mer)] and $[Ru^{III}(NH_3)_5$-H21(30-mer)] peptides in 50 mM phosphate buffer (pH 7.0) over zinc amalgam under an argon atmosphere. Measured quantities of the stock solution were then transferred via Hamilton Gastight syringes and diluted to the desired peptide concentration by addition to a N_2O-saturated, 1 mM NaN_3, 50 mM pH 7.0 phosphate buffer solution in the radiolysis cell. In most cases, the peptide samples were prepared with 1−2 equivalents of an exogenous reductant, Eu_{aq}^{2+}, per equivalent of $[Ru(NH_3)_5$-H21(30-mer)]. This reductant was added to keep the sample in its reduced state prior to the application of the radiolytic dose.[29] However, under such conditions, the europous ion can act to intercept the radiolytically generated azide radical. This interception would result in decreasing the absolute yield of the Ru^{III}-(trpy)(bpy)-peptide, as evidenced by the observation of a smaller absorption bleach than would be seen in the absence of the reductant. The Eu^{2+} species can also react with the radiolytically generated Ru^{III}-(trpy)(bpy)-peptide to produce an observed recovery of the absorption bleach that is faster than the true intramolecular ET rate. Thus, the kinetic experiments were performed in such a manner as to eliminate the Eu^{2+} species in situ before the desired intramolecular ET rate was measured. Successive radiolytic doses were therefore applied to a given peptide sample to oxidatively titrate the Eu^{2+} species until (1) the initial bleach at 490 nm had grown to the value initially observed in the absence of europous ion, and (2) the observed recovery rate had decreased to a constant value over several successive shots.

Circular Dichroism Measurements. Circular dichroism (CD) spectra were obtained with an Aviv and Associates model 62DS CD spectrometer (Lakewood, NJ) equipped with a thermoelectric temperature controller. A rectangular 1-mm path length cell was used (sample volume ≤ 400 μL). The spectrometer was routinely calibrated with an aqueous solution of (1*S*)-(+)-10-camphorsulfonic acid. Mean residue molar ellipticities were calculated according to the following equation:

$$[\theta] = [\theta]_{obs}/(10^\bullet\ lcn) \qquad (4)$$

where $[\theta]_{obs}$ is the observed ellipticity measured in degrees, l is the path length of the cell in centimeters, c is the molar peptide concentration, and n is the number of amino acid residues in the peptide. The spectra were obtained as an average of 3−5 scans using a wavelength step of 1 nm. The thermal denaturation results were obtained by measuring the ellipticity at 222 nm as a function of temperature using a six-second thermal equilibration time between data points. The series of solutions used in the concentration studies were prepared by serial dilution of a concentrated stock solution prepared from dissolving a known mass of the lyophilized peptide into a known volume phosphate buffer (pH 7.0). The values reported for K_d and θ_{max} are taken from an average of two separate experiments.

Gel Electrophoresis and Chemical Cross-Linking Experiments. Discontinuous polyacrylamide gel electrophoresis (PAGE) was performed on samples of the closely related peptide, Ru(bpy)$_2$Im-H21-(31-mer),[21] dissolved in HEPES buffer in the absence of sodium dodecyl sulfate (pH 7.0) at either room temperature or after heating to 80 °C for 15 min prior to loading. Experiments were performed in the presence of SDS (0.1% v/v) in the running buffer at 200 V for 45 min. The molecular mass standards for aprotinin (6 kDa), plastocyanin (10 kDa), lysozyme (14 kDa), and cytochrome *c* (21 kDa) were run in parallel for comparison.

Nonspecific intersubunit cross-linking was performed on samples of the metalloheterodimer using glutaraldehyde as the linker.[30] Glutaraldehyde reacts with the free amine groups at the N-terminal of the peptide and at the lysine residues. Mixtures containing equal molar amounts of [Ru(bpy)$_2$Im-H21(31-mer)] and [Ru(NH$_3$)$_5$-H21(31-mer)] were dissolved in 50 mM phosphate buffer, heated to 80 °C for 30

(28) (a) Sullivan, B. P.; Calvert, J. M.; Meyer, T. J. *Inorg. Chem.* **1980**, *19*, 1404. (b) Ware, D. C.; Lay, P. A.; Taube, H. *Inorg. Synth.* **1986**, *24*, 299. (c) Johnson, E. C.; Sullivan, B. P.; Salmon, D. J.; Adeyemi, S. A.; Meyer, T. J. *Inorg. Chem.* **1978**, *17*, 2211.

(29) Sun, J.; Su, C.; Wishart, J. F. *Inorg. Chem.* **1996**, *35*, 5893.

(30) Habeeb, A. F.; Hiramoto, R. *Arch. Biochem. Biophys.* **1968**, *126*, 16.

min, and then allowed to cool back to room temperature before the addition of glutaraldehyde (final concentrations ranged from 2 to 100 mM). The samples were incubated at 37 °C for 20 min before being quenched by adding glycine to a final concentration of 100 mM. These samples were then run on an 18% SDS-PAGE gel. Two different polypeptide standards were run in parallel (3.4, 5.5, 8.7, and ≥15.3 kDa; 3.0, 5.0, 9, and ≥14 kDa) for comparison.

Analytical Ultracentrifugation. Sedimentation equilibria were determined for samples of the [Ru(bpy)$_2$Im-H21(31-mer)]/[Ru(NH$_3$)$_5$-H21(31-mer)] heterodimer[21] using a Beckman Optima XL-A ultracentrifuge run at 50 000 rpm for 24 h at 25 °C. The sample was prepared as already described with an initial concentration of ∼50 μM. The partial specific volume was estimated to be 0.74 cm^3 g^{-1} from peptide composition,[31] with a correction made for the ruthenium complex. The solvent density was taken to be 1.002 g cm^{-3}.[32] Data were obtained from four different runs and averaged.

Electron Paramagnetic Resonance (EPR) Spectroscopy and Spectral Analysis. EPR spectra were collected with a Bruker ESP 300E spectrometer (Bruker, Germany) equipped with a loop-gap resonator (Medical Advances, Milwaukee, WI) and a low-noise microwave amplifier (Miteq, Hauppauge, NY). Spin concentrations were determined by comparing doubly integrated room-temperature spectra with that of a TEMPO standard solution. Low-temperature spectra were collected at 125 K at 8-microwatt microwave power and a modulation amplitude of 1 G, and spin concentration was ∼300 μM. The EPR spectra were independent of concentration up to 2 mM.

Electron dipolar interactions between two interacting nitroxide spin labels lead to overall EPR spectral broadening. Quantitative analysis of room-temperature spectra is nontrivial because of the motional line broadening in addition to the dipolar line broadening. Low-temperature spectra of motionally frozen samples permits extraction of the dipolar broadening function directly from Fourier deconvolution analysis of the interacting double-label spectra with respect to noninteracting monoradical spectra.[33] The motionally frozen state is readily achieved by freezing the EPR samples near the liquid nitrogen temperature. This method provides an accurate estimation for interspin distances in the range 8−25 Å, and its applications to peptides and proteins have been described previously.[34−36]

Because these experiments were designed to detect the relatively weak dipolar interactions between two spin labels at the *f* positions of the peptide dimer, which are >20 Å apart, special efforts were made to minimize the experimental error. The average of five independently obtained low-temperature spectra was used in the final analysis. The noninteracting monoradical reference spectra were taken both from the sample prepared by mixing the spin-labeled peptide with the unlabeled peptide at a 1:10 mole ratio and from a sample of the spin-labeled peptide sample denatured in 6 M GuHCl.

Molecular Modeling. Computational results were obtained using software programs from Biosym/MSI (San Diego, CA). Energy minimization calculations were performed with the *Discover*® program using the ESFF force field and the conjugate gradient method, setting a final convergence criterion of 0.001 kcal/(mol Å) rms force. Molecular dynamics simulations were performed by the Nose temperature control method. All structures were solvated with a water box prior to performing the calculations. Graphical displays were obtained from the *Insight*®*II* molecular modeling program.

Results

Synthesis and Characterization of Peptides. Solid-phase methods were used to prepare a 30-residue polypeptide called H21(30-mer). The sequence (Ac−K(IEALEGK)$_2$(IEALE**H**K)-(IEALEGK)G-NH$_2$) was based on a seven-residue repeat developed by Hodges and co-workers to prepare artificial coiled-coils.[25] In the sequence, positions *a*, *d*, *e*, and *g* are occupied by isoleucine, leucine, glutamic acid, and lysine, respectively, as these substitutions have been shown to encourage the formation of two-stranded coiled-coils in solution. In particular, it has been found that dimeric coiled-coils are favored by the incorporation of β-branched amino acids into position *a* of the heptad. An additional feature of the sequence is that it places a single histidine residue at position 21 to provide a metal-binding site on the most highly solvent-exposed position of the third heptad repeat.

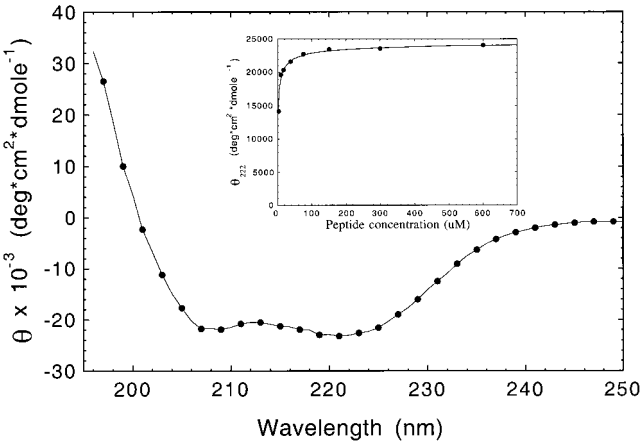

Figure 2. The circular dichroism spectrum of a 76 μM solution of H21(30-mer) peptde in 50 mM phosphate buffer (pH 7, 298 K). Inset: The concentration dependence of θ_{222} for H21(30-mer). The solid line shows the fit to a two-state monomer−dimer equilibrium model (eq 6) as described in the text.

The two metallopeptides, [Ru(trpy)(bpy)-H21(30-mer)] and [Ru(NH$_3$)$_5$-H21(30-mer)], were prepared by appropriate modification of methods previously described for the attachment of ruthenium complexes to the surface of cytochrome *c*.[6c,27] In each case, purification was achieved by a combination of semi-preparative reversed-phase HPLC and size-exclusion chromatography. The UV absorption spectrum of the [Ru(trpy)(bpy)-H21(30-mer)] peptide exhibits maxima at λ = 206 (log ϵ = 5.0), 274 (log ϵ = 4.5), 288 (log ϵ = 4.5), 314 (log ϵ = 4.50), and 476 nm (log ϵ = 3.9), and is quite similar to the spectrum previously reported for the related model compound, [Ru(trpy)-(bpy)Im]$^{2+}$.[27b] When dissolved in water, the metallopeptide has a short-lived emission at 650 nm (τ = 23 ns) that is nearly the same as that reported for the related ruthenated plastocyanin.[27] Differential pulse polarography and CV show a reversible redox couple for the metallopeptide at $E_{1/2}$ = +1.17 V versus NHE that is similar to the value reported for the model compound, [Ru$^{3+/2+}$(trpy)(bpy)Im].[27,37] Characterization of the [Ru(NH$_3$)$_5$-H21(30-mer)] peptide was accomplished by CV, which showed nearly identical behavior to that of Ru(NH$_3$)$_5$-modified cytochrome *c*.[6c] A reversible one-electron reduction at $E_{1/2}$ = +0.065 V versus NHE was observed.

Circular Dichroism Spectroscopy. Figure 2 shows the circular dichroism (CD) spectrum of a 76 μM solution of H21-(30-mer) in 50 mM phosphate buffer (pH 7, 298 K). The spectrum consists of a positive signal located below 200 nm, and a pair of negative signals at 208 and 222 nm, which demonstrates the existence of an α-helical structure. At the concentrations used for the ET measurements described later,

(31) McMeekin, T.L.; Groves, M. L.; Hipp, N. J. *J. Am. Chem. Soc.* **1949**, *71*, 3298.

(32) Weast, R. C. *Handbook of Chemistry and Physics*; CRC Press: Boca Raton, FL, 1985.

(33) Rabenstein, M. D.; Shin, Y.-K. *Proc. Natl. Acad. Sci., U.S.A.* **1995**, *92*, 8239.

(34) Hall, J. A.; Thorgeirsson, T. E.; Liu, J.; Shin, Y.-K.; Nikaido, H. *J. Biol. Chem.* **1997**, *272*, 17 610.

(35) Thorgeirsson, T. E.; Xiao, W.; Brown, L. S.; Needleman, R.; Lanyi, J. K.; Shin, Y.-K. *J. Mol. Biol.* **1997**, *273*, 951.

(36) Ottemann, K. M.; Thorgeirsson, T. E.; Kolodziej, A. F.; Shin Y.-K.; Koshland, D. E. *Biochemistry* **1998**, *37*, 7062.

(37) A second reversible wave seen at 0.87 V versus NHE is assigned to the presence of [Ru$^{3+/2+}$(trpy)(bpy)(H$_2$O)] which is observed as a minor component (<5%) by HPLC in the peptide sample.

an ellipticity ratio of $\theta_{222}/\theta_{208} = 1.06$ was observed, which indicates the existence of an α-helical coiled-coil.[25] In contrast, single-stranded α-helices are expected to display values of $\theta_{222}/\theta_{208} \approx 0.86$, as theoretical calculations have shown that the CD band located at 208 nm is polarized parallel to the helical axis and its magnitude is therefore sensitive to whether the helical structure is comprised of a single peptide chain or interacting α-helices.[38] It is interesting to note that when H21(30-mer) is dissolved in methanol, $\theta_{222}/\theta_{208} = 0.9$, indicating that the coiled-coil structure has unfolded into noninteracting helical monomers. Thermal denaturation studies performed in aqueous solution (not shown) indicate that the self-assembled peptide structure is very stable, producing a melting curve in which $T_m = 65$ °C.

The ellipticity value at 222 nm can be used to estimate the helical content of the peptide by comparison to the maximum molar ellipticity (X_H^∞) calculated for a 30-residue polypeptide:

$$X_H^\infty = (-37\,400 \text{ deg cm}^2 \text{ dmol}^{-1})(1 - k/n) = -34\,283 \text{ deg cm}^2 \text{ dmol}^{-1} \quad (5)$$

where k is a wavelength-dependent constant equal to 2.5 at 222 nm, and n is the number of residues per helix.[39] Significantly, the observed helicity of the H21(30-mer) peptides increases with increasing peptide concentration, which is consistent with the formation of a self-assembled coiled-coil structure. Recent studies[40] of some coiled-coil peptides have analyzed the concentration dependence of θ_{222} in terms of a two-state monomer−dimer equilibrium for which the dissociation constant, K_d, can be calculated from eq 6:

$$K_d = 2[M_0]\,(1 - \Delta\theta/\Delta\theta_{max})^2/(\Delta\theta/\Delta\theta_{max}) \quad (6)$$

where $[M_0]$ is the total peptide concentration, $\Delta\theta = (\theta_{obs} - \theta_0)$, $\Delta\theta_{max} = (\theta_{max} - \theta_0)$, θ_{max} is the ellipticity of the folded dimer, and θ_0 is the ellipticity of the unfolded monomer, which is usually taken to be 2500 deg cm^2 dmol^{-1}. All ellipticities are at 222 nm. The inset in Figure 2 shows the results of a nonlinear least-squares fit of the concentration dependence of θ_{222} to eq 6, which yields values of $K_d = 1.5 \pm 0.4$ μM and $\theta_{max} = -23\,800 \pm 130$ deg cm^2 dmol^{-1}, showing that the peptide has a maximum helicity of 69%. These results are consistent with those reported for studies[25] of synthetic coiled-coils with similar amino acid sequences to that of H21(30-mer) in which the deviations from ideality are likely due to endgroup fraying.

The CD properties of the [Ru(trpy)(bpy)-H21(30-mer)] and [Ru(NH$_3$)$_5$-H21(30-mer)] metallopeptides are qualitatively similar to those of the apopeptide. Both show a positive CD band at <195 nm and two minima at 208 and 222 nm. In addition, both peptides display values of $\theta_{222}/\theta_{208} = 1.05$, indicating that they adopt the coiled-coil structure when dissolved in aqueous solution. The concentration dependence of θ_{222} for the two metallopeptides can be fit to eq 6 to give $K_d = 0.27 \pm 0.1$ μM and $\theta_{max} = -19\,031 \pm 76$ deg cm^2 dmol^{-1} for the [Ru(NH$_3$)$_5$-H21(30-mer)] and $K_d = 0.24 \pm 0.1$ μM and $\theta_{max} = -26\,176 \pm 114$ deg cm^2 dmol^{-1} for the [Ru(trpy)(bpy)-H21(30-mer)].

Gel Electrophoresis, Chemical Cross-Linking Experiments, and Analytical Ultracentrifugation. SDS-PAGE experiments (not shown) were used to determine the oligomerization state of the H21(30-mer) and showed the presence of monomers and dimers in solution. Subsequent intersubunit cross-linking experiments using glutaraldehyde also produced bands at positions corresponding to the monomer and dimer species (MW < 8.7 kDa). Higher concentrations of glutaraldehyde produced more intense dimer bands. However, no evidence for higher cross-linked oligomers was observed, even under saturating conditions of glutaraldehyde. To directly determine the molecular weight of the peptide in solution, the sedimentation equilibrium of equimolar samples of the [Ru(bpy)$_2$Im-H21(31-mer)] and [Ru(NH$_3$)$_5$-H21(31-mer)] metallopeptides were studied by analytical ultracentrifugation. Figure 3 shows that the results obtained within the concentration range 20−80 μM can be accurately fit to a dimer model using the averaged molecular weight of 7.5 kDa for the dimer. Metal derivatization of the peptide does not seem to perturb its overall aggregation state as was sometimes observed in the case of organic fluorophores attached to coiled-coil peptides.[41]

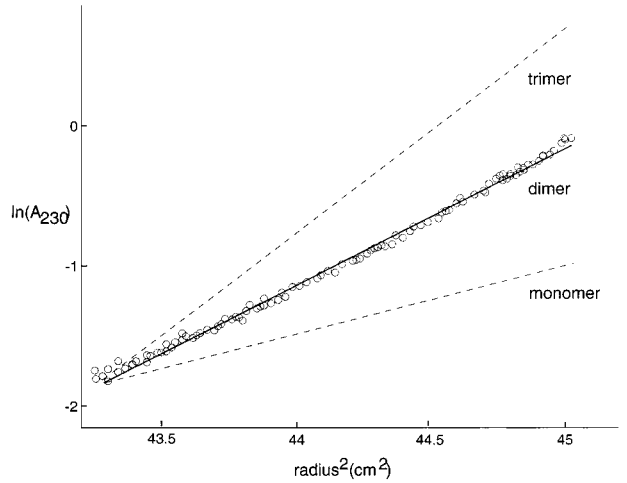

Figure 3. Determination of the molecular weight of the Ru(bpy)$_2$Im-H21(30-mer)/Ru(NH$_3$)$_5$-H21(30-mer) peptide sample by sedimentation equilibrium ultracentrifugation. The observed data can be fit to a dimeric model (solid line).

Preparation of the ET Metallo-heterodimer. The results just discussed show that the two noncovalent metallohomodimers, [Ru(trpy)(bpy)-H21(30-mer)]$_2$ and [Ru(NH$_3$)$_5$-H21(30-mer)]$_2$, can be readily prepared. In a recent study of a related peptide, stopped-flow CD spectroscopy was used to examine the unfolding kinetics of a dimeric coiled-coil peptide to yield a half-life of several minutes.[42] Thus, the desired ET heterodimer (Figure 4) was generated in situ by mixing an approximately equimolar solution of the two homodimers and allowing the sample to stand under ambient conditions for at least 25 min. This procedure yields a statistical mixture of the peptide homodimers and heterodimers that cannot be separated from one another. However, we note that within this statistical distribution of metallopeptides, the [Ru(trpy)(bpy)-H21(30-mer)]/[Ru(NH$_3$)$_5$-H21(30-mer)] heterodimer is the only species that can display intracomplex ET.

EPR Measurements. The nitroxide−nitroxide distance measured by EPR was used to estimate the distance between the two α-carbons at positions 21 and 21′ within the peptide dimer. These positions are the sites of ruthenium attachment in the ET metalloprotein already described. The identity of the spin-labeled variant was verified by ESI-MS and its dimeric aggregation state was confirmed by analytical ultracentrifugation.

Figure 5a shows a comparison of the average of five independently obtained spectra of the [MTSL-C21(30-mer)]$_2$

(38) Cooper, T. M.; Woody, R. W. *Biopolymers* **1990**, *30*, 657.
(39) Chen, Y.-H.; Yang, J. T.; Chau, K. H. *Biochemistry* **1974**, *13*, 3350.
(40) Wendt, H.; Berger, C.; Baici, A.; Thomas, R. M.; Bosshard, H. R. *Biochemistry* **1995**, *34*, 4097.
(41) Daugherty, D. L.; Gellman, S. H. *J. Am. Chem. Soc.* **1999**, *121*, 4325.
(42) Zitzewitz, J. A.; Bilsel, O.; Luo, J.; Jones, B. E.; Matthews, C. R. *Biochemistry* **1995**, *34*, 12812.

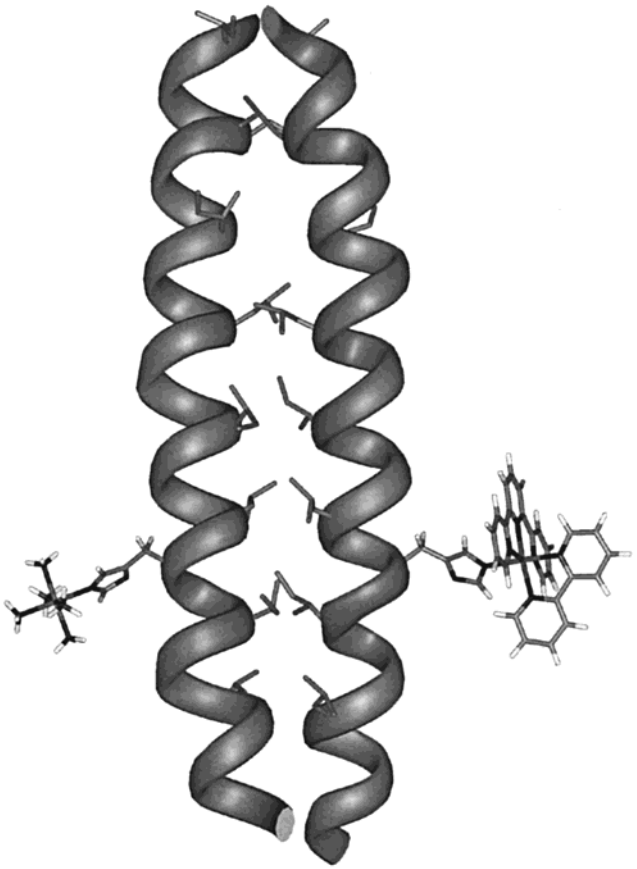

Figure 4. Computer-generated model of the heterodimer electron-transfer metalloprotein.

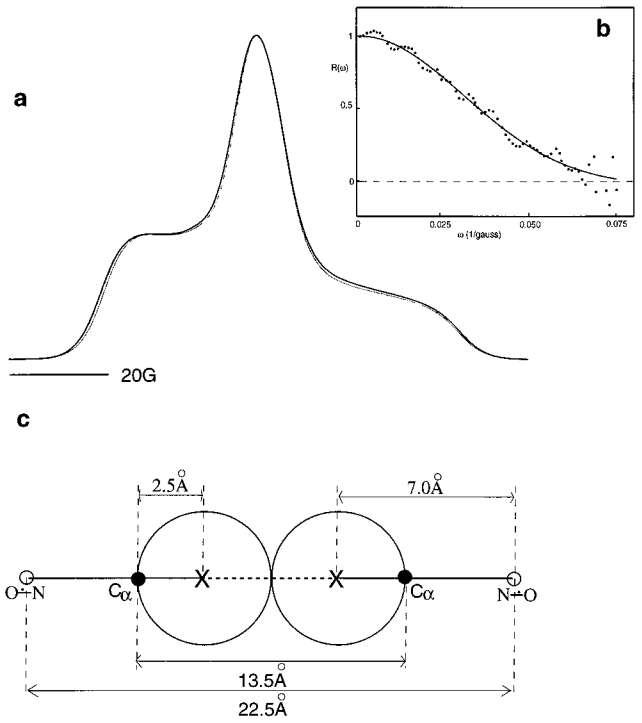

Figure 5. EPR measurements of the interspin distance and modeling of the helical geometry. (a) The low-temperature absorbance spectrum for the [MTSL-C21(30-mer)]$_2$ peptide dimer (thick line), overlapped with the noninteracting spectrum from the wild-type titration experiment (thin line) and from the GuHCl denaturation experiment (dashed line). (b) The broadening function due to interspin dipolar interaction shown in Fourier space (dots) and the fit to a two-Gaussian to eliminate random noise (solid line). (c) Model of the peptide dimer with nitroxide spin labels at the *f* positions. Helix wheels of the peptide dimer are shown as two circles, with the center of the helix (*X*), the C_α position (Cα), and the averaged nitroxide position (N−O).

dimer, with the noninteracting spectra obtained from a magnetically dilute sample of [MTSL-C21(30-mer)] dissolved in a stoichiometric excess of unmodified [C21(30-mer)], and a sample of [MTSL-C21(30-mer)] denatured in 6 M GuHCl. This comparison reveals a small but distinct spectral line broadening in the spin-labeled dimer due to electron−electron dipolar interactions. Importantly, no evidence for the presence of monomeric peptides was detected in these samples.

Fourier deconvolution analysis was performed to determine the interspin distance from these spectra. Previous studies have measured interspin distances in derivatized α-helices to show that the experimentally determined values were identical to those calculated from idealized models within a standard deviation of ±0.9 Å.[33] The dipolar broadening function extracted from the analysis in the Fourier space is shown in Figure 5b. From this function, an average interspin distance of 22.5 Å was obtained. These results were invariant to the choice of reference sample used to compare the line shapes (i.e., the magnetically diluted, or chemically denatured samples).

An estimate of the intersubunit $C_\alpha(21)-C_\alpha(21')$ distance can be obtained from the spin-label distance using the following geometrical argument (Figure 5c). In several previous studies, it has been found that the average location of a nitroxide spin-label attached to an α-helix lies 7 Å away from the center of the helix on the line connecting the helical axis and the α-carbon of the cysteine residue.[33,43] The C_α positions are located 2.5 Å away from the helical axis along this radius. Thus, the two C_α sites at the *f* positions of the dimer lie nearly on the straight line connecting the two helical axes. The distance between these sites is therefore measured to be 13.5 ± 0.9 Å, which is within experimental error to the average value of 14.2 Å seen in the 1.8 Å resolution crystal structure of GCN-4.[44] The H21(30-mer) is therefore believed to exist within the nativelike structure of an α-helical coiled-coil. These results also indicate that the peptide dimer consists of a parallel arrangement of α-helices because an antiparallel arrangement would result in very large interspin distances giving rise to narrow EPR signals.

Molecular Modeling. As described later, the pulse radiolysis technique was used to determine the rates of a ground-state ET occurring from the $Ru^{II}(NH_3)_5$ electron-donor (d^6) to the Ru^{III}-(trpy)(bpy) acceptor (d^5). Because this reaction involves metal-based d-orbitals, an estimate of the metal-to-metal distance in the ET heterodimer was obtained by energy-minimization calculations based on the results previously obtained[45] for the related metalloheterodimer [Ru(bpy)$_2$Im-H21(31-mer)]/[Ru-$(NH_3)_5$-H21(31-mer)] whose synthesis has been described earlier.[21] These calculations were initiated by coordinating the appropriate ruthenium complexes to the H21 positions of the 31-mer apopeptide using starting coordinates taken from the crystal structures of the GCN-4 dimerization domain,[44] and the relevant model complexes, *cis*-[Ru(bpy)$_2$Im$_2$](BF$_4$)$_2$[46] and [$(NH_3)_5$-Ru(His)]Cl$_3$•H$_2$O.[47] Separate energy minimization calculations were then performed for 640 initial structures in which the side-

(43) Macosko, J. C.; Kim, C. H.; Shin, Y.-K. *J. Mol. Biol.* **1997**, *267*, 1139.

(44) O'Shea, E. K.; Klemm, J. D.; Kim, P. S.; Alber, T. *Science* **1991**, *254*, 539.

(45) Unpublished results.

(46) Reddy, K. B.; Cho, M. P.; Wishart, J. F.; Emge, T. J.; Isied, S. S. *Inorg. Chem.* **1996**, *35*, 7241.

(47) Krogh-Jespersen, K.; Westbrook, J. D.; Potenza, J. A.; Schugar, H. J. *J. Am. Chem. Soc.* **1987**, *109*, 7025.

Scheme 1

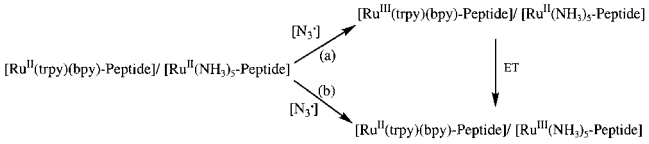

chain dihedral angles χ_1 and χ_2 for the H21 residue were systematically varied from $-180°$ to $+180°$ and in which the backbone structure of the peptide remained fixed. For the current study, the two lowest energy structures were identified, and their ruthenium polypyridyl sites were changed to [Ru(trpy)(bpy)]. Energy minimization calculations were subsequently performed followed by molecular dynamics simulations at 298 K to overcome local energy barriers. After a second round of energy minimization was performed an average metal-to-metal distance of 24.4 Å was found, which was within 0.2 Å of the value obtained from the original starting coordinates. From these final coordinates, the edge-to-edge distance is 18.4 Å as measured from the C_γ positions of the histidine residues.

Electron-Transfer Studies. The monitoring wavelength for studying the ET kinetics was determined by examining the difference absorption spectra obtained after oxidizing the [Ru^{II}-(trpy)(bpy)-H21(30-mer)] peptide with $N_3^\bullet$ radical. Correction for the radiolytic yield permits calculation of the differential extinction coefficient at each observed wavelength (data not shown), and the largest absorption bleach was seen to occur at 490 nm ($\Delta\epsilon = -5980\ M^{-1}\ cm^{-1}$).

The kinetics of the intramolecular ET reaction occurring within the [Ru(trpy)(bpy)-H21(30-mer)]/[$Ru(NH_3)_5$-H21(30-mer)] heterodimer was measured by pulse-radiolysis, as shown in Scheme 1. In this experiment, the radiolytically generated azide radical was used to oxidize either of the two ruthenium centers in the reduced heterodimer to create a nonequilibrium distribution of the two singly oxidized species. Electron transfer brings the system back to redox equilibrium in a process that can be followed by transient optical absorption. The ET measurements were carried out on solutions having concentrations in the range of 1.2 to 20 μM for the heterodimer (total peptide concentrations of 2.4 to 40 μM).[48] Control experiments were performed on similar solutions of the [Ru(trpy)(bpy)-H21-(30-mer)] homodimer. The usable concentration range for these experiments was limited on the low end by the monomer−dimer equilibrium constant, and at the high end by the absorbance of the sample.

Figure 6a shows a typical transient absorption trace from a control experiment involving the pulse radiolysis of [Ru(trpy)-(bpy)H21(30-mer)] (total peptide concentration = 10 μM). A rapid bleach at 490 nm is observed that indicates formation of the oxidized [Ru^{III}(trpy)(bpy)H21(30-mer)] species. The second-order rate constant for this process is $k_{ox} \approx 1.5 \times 10^9\ M^{-1}\ s^{-1}$, based on the pseudo-first-order rate constants measured at different peptide concentrations. As shown, the oxidized met-allopeptide lives for >70 ms in the absence of a reductant. Observations at longer times show evidence for a partial (~20%) recovery of the MLCT bleach occurring within ~1000 ms.

Figure 6b shows the results of the radiolysis experiment performed on a 5.2-μM solution of the ET heterodimer

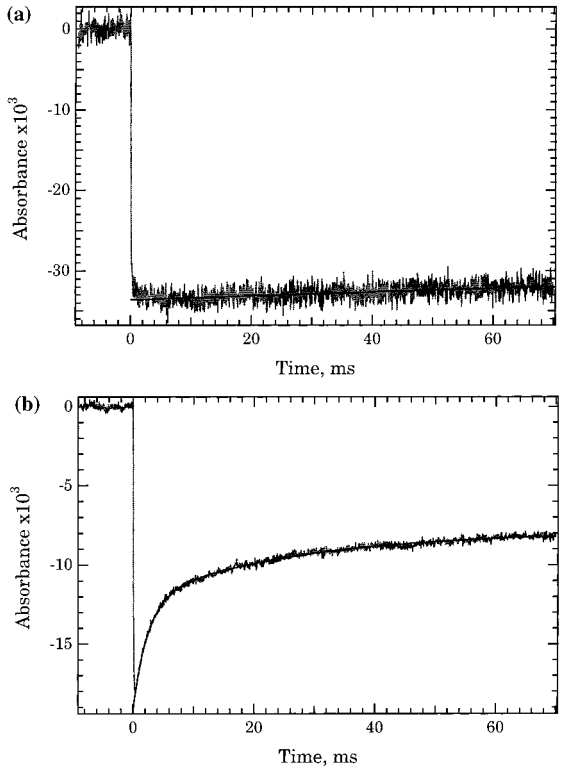

Figure 6. (a) Transient absorption plot obtained at 490 nm for the pulse radiolysis of a 5-μM solution of the [Ru^{II}(trpy)(bpy)-H21(30-mer)] peptide in a N_2O-saturated solution containing 1 mM NaN_3 and 50 mM phosphate buffer at pH 7. A tungsten lamp was used as the source of the analyzing beam. (b) Transient absorption plot obtained at 490 nm for the pulse radiolysis of a 5.2-μM solution of the [Ru-(trpy)(bpy)-H21(30-mer)]/$Ru^{II}(NH_3)_5$-H21(30-mer)] ET heterodimer (total peptide concentration = 10.4 μM) in a N_2O-saturated solution containing 1 mM NaN_3 and 50 mM phosphate buffer at pH 7. A pulsed xenon arc lamp was used as the source of the analyzing beam.

preparation (total peptide concentration of 10.4 μM). A rapid bleach is observed at 490 nm that indicates that the ruthenium polypyridyl centers have been oxidized by the azide radical. This process proceeds with an estimated second-order rate constant of $\sim k_{ox} = 2 \times 10^9\ M^{-1}\ s^{-1}$, which is similar to that already seen for the oxidation of the related homodimer. However, the absorption change observed for the ET heterodimer recovers by a process that can be fit to a sum of two exponentials within the 70-ms time scale of the experiment. The rate of the faster major component is independent of concentration, and is thus assigned to the intracomplex ET reaction. Measurements were performed on samples containing 1.2, 2.0, 4.0, 5.2, 10, and 20 μM solutions of the ET heterodimer to give first-order rate constants of $k_{et} = 290 \pm 60$ (12), 410 ± 50 (11), 400 ± 35 (9), 400 ± 50 (12), 480 ± 40 (11), and $310 \pm 50\ s^{-1}$ (9), respectively, where the number of independent observations made for each concentration are shown in parentheses. These data give an average value of $k_{et} = 380 \pm 80\ s^{-1}$ for the intramolecular ET reaction occurring within the ET heterodimer. This value supersedes the one previously reported for a closely related peptide,[21] in which the laser flash quench method was improperly used because of the incorrect choice of the exogeneous quencher that allowed for the pre-flash oxidation of the donor site.[49]

Examination of Figure 6b also shows the existence of a persistent bleach at 490 nm. This behavior is similar to that seen in Figure 6a and can be attributed to the radiolytic oxidation of the [Ru^{II}(trpy)(bpy)-H21(30-mer)] homodimers present in the solution (these account for half of the [Ru^{II}(trpy)(bpy)] species

(48) Samples of the ET heterodimer were obtained from a total of seven independent preparations of peptide. Samples from six of these preparations displayed consistent kinetic behavior that is described in the text. The samples obtained from the remaining preparation displayed much faster kinetics appearing on the submillisecond time scale. However, these kinetics were observed for an initial MLCT bleach that was an order of magnitude smaller than that expected from comparison with the behavior seen for the [Ru(trpy)(bpy)-H21(30-mer)] homodimer ($-\Delta\epsilon = 3$ to $6 \times 10^2\ M^{-1}\ cm^{-1}$), and are therefore ascribed to the presence of an unidentified reductant in solution.

present), as well as to the accumulation of the ET-inert product, $[Ru^{II}(trpy)(bpy)\text{-}H21(30\text{-}mer)]/[Ru^{III}(NH_3)_5\text{-}H21(30\text{-}mer)]$. These oxidized ruthenium polypyridyl species can only decay by a bimolecular ET reaction with the a $[Ru^{II}(NH_3)_5\text{-}H21(30\text{-}mer)]$ species. However, only a small percentage can react in this way because the concentration of the ruthenium(II) pentammine sites has been lowered by repeated pulsing of the sample. The kinetic fits to the data show that the slower, minor component to the bleach recovery appears to occur with a concentration-independent rate of $k_{apparent} = 32 \pm 9\ s^{-1}$. However, the small amplitude of this component and the 70-ms time domain of the experiment prevents an unambiguous analysis of these data to be made at this time.

Discussion

This work describes a new approach toward the preparation of self-assembled peptide complexes that are capable of displaying long-range ET reactions. In recent years, several examples have been reported in which the principles of de novo protein design have been used to prepare a new generation of synthetic ET proteins.[22−24] However, a unique feature of the current system is that instead of using polypeptide chains to provide covalent bridges between the electron donor and acceptor sites, the ET event is now made to occur across a well-defined, yet noncovalent, peptide−peptide interface. Accordingly, this synthetic protein provides the first peptide-based model system that is amenable to mechanistic studies of interfacial ET reactions as they occur within native protein−protein complexes.

The results of CD, EPR, analytical ultracentrifugation, and molecular modeling studies show that both the apo and metalated derivatives of the [H21(30-mer)] peptide form two-stranded α-helical coiled coils that remain essentially isostructural to the family of native leucine zipper proteins. In particular, the EPR spin-label experiments show that the interchain C21−C21′ distance ($C_\alpha - C_\alpha$) of the peptide dimer is nearly identical to that observed from the X-ray crystal structure of GCN-4. Based on these results, computer modeling studies suggest that the ET heterodimer, $[Ru(trpy)(bpy)\text{-}H21(30\text{-}mer)]/[Ru(NH_3)_5\text{-}Im\text{-}H21(30\text{-}mer)]$, has an interhelix, metal-to-metal distance of ∼24 Å.

Pulse radiolysis experiments were used to measure a concentration-independent value of $k_{et} = 380 \pm 80\ s^{-1}$ for the interhelix ET reaction occurring between the $[Ru^{II}(NH_3)_5H21(30\text{-}mer)]$ electron-donor and the $[Ru^{III}(bpy)(trpy)H21(30\text{-}mer)]$ acceptor.

The electrochemistry measurements performed on the two metallo-homodimers show that the driving force for this reaction is $\Delta G^\circ = -1.11$ eV, which is slightly higher than the magnitude of λ calculated for this system.[50] The observed value of k_{et} is therefore believed to be close to that of k_{max} (i.e., the activationless ET rate constant) and can therefore be compared with those reported for related systems. Interestingly, the value falls within the range of those reported for ET reactions that occur across comparable metal-to-metal distances in both native and surface-modified metalloproteins. For example, Farver and Pecht[51] report a value of $k_{max} = 3 \times 10^2\ s^{-1}$ for the reaction between the $[Cys3\text{-}S-S\text{-}Cys26]^{\bullet -}$ disulfide radical and the Cu^{2+} center of wild-type azurin that are located 24.6 Å apart. In addition, Gray and co-workers[4b] report values of $k_{max} = 3.1 \times 10^4\ s^{-1}$ for His54-ruthenated cytochrome *c* ($d_{M-M} = 22.5$ Å), $k_{max} = 2.4 \times 10^2\ s^{-1}$ for His107-ruthenated azurin for ($d_{M-M} = 25.7$ Å), and $k_{max} = 1.3 \times 10^2\ s^{-1}$ for His126-ruthenated azurin ($d_{M-M} = 26$ Å). The behavior of the H21(30-mer) metalloprotein clearly falls within this range of data and highlights the rich variability in the ET behavior of protein-based systems.

At this point, it should be acknowledged that relatively little is presently known about the conformational dynamics of the ET heterodimer. It is certainly possible that internal motions of the metalloprotein may play an important role in regulating the observed intracomplex ET rate. However, it appears likely that the gross dynamics of the monomer/dimer equilibrium do not gate the observed ET reaction because Zitzewitz et al.[42] recently used stopped-flow CD to determine that the monomer/dimer equilibrium for the related GCN-4 coiled-coil peptide has an unfolding rate constant of $3.3 \times 10^{-3}\ s^{-1}$, which is significantly smaller than the ET rate constant measured in the present system. Nevertheless, future work will attempt to address this issue by examining the temperature and/or viscosity dependence of k_{et} for this and related systems. In the absence of such experiments, a pathway analysis of the H21(30-mer) ET heterodimer identifies the primary coupling path (metal-to-metal) in this system to consist of 22 covalent bonds and a critical interhelix through-space jump of 3 Å between the C_β of Lys22 and C_γ of Ile23′ of the next heptad repeat.[52] Interestingly, a secondary pathway is also identified that has the same number of covalent interactions and only a 20% lower coupling strength than that of the primary path because of a slightly longer through-space jump occurring between the C_α of Glu20 and the C_δ of Leu19′. Thus, ongoing work in our laboratory is attempting to chemically modify the nature of the peptide−peptide interface to probe the mechanisms of interfacial ET reactions.

Acknowledgment. The authors thank Professor George S. Bullerjahn for many helpful discussions. This work was partially supported by the Petroleum Research Fund administered by the American Chemical Society (M.Y.O.) and by the National Institutes of Health through grant nos. GM61171 (M.Y.O.) and GM51290 (Y.K.S.). The pulse radiolysis experiments were carried out at Brookhaven National Laboratory under contract DE-AC02-98CH10886 with the U.S. Department of Energy and supported by its Division of Chemical Sciences, Office of Basic Energy Sciences. Support from the National Science Foundation is acknowledged for the purchase of the circular dichroism spectrometer at BGSU through grant no. BIR-9208356. A.Y.K. and A.F. thank the Harold and Helen McMaster Foundation for predoctoral fellowships. R.C.L. acknowledges support from a George S. Hammond predoctoral fellowship from the Center for Photochemical Sciences at BGSU.

JA0006954

(49) Our studies have also found that the $Ru(bpy)_2(im)\text{-}H21(31\text{-}mer)$ homodimer used in the previous study is photolabile in the absence of quencher. Photoexcitation of this species results in a transient bleach of the ruthenium MLCT peak, which does not fully recover to the original baseline on the millisecond time scale.

(50) An estimate of the reorganization energy for this system can be made using the Marcus cross-relation: $\lambda_{12} = 1/2\ [\lambda_{11} + \lambda_{22}]$ where λ_{11} and λ_{22} are the self-exchange reorganization energies for two metal complexes involved in the electron−transfer. Substitution of the values (ref 4c) of $\lambda_{11} = 0.6$ eV for $Ru(bpy)_3$, and $\lambda_{22} = 1.20$ eV for $Ru(NH_3)_5$ (pyr) yields a value of $\lambda_{12} = 0.9$ eV.

(51) Farver, O.; Skov, L. K.; Gilardi, G.; van Pouderoyen, G.; Canters, G. W.; Wherland, S.; Pecht, I. *Chem. Phys.* **1996**, *204*, 271.

(52) Kurnikov, I.; Beratan, D. N., private communication.